Atmos. Chem. Phys. Discuss., 11, 32161–32204, 2011
www.atmos-chem-phys-discuss.net/11/32161/2011/
doi:10.5194/acpd-11-32161-2011

Atmospheric Chemistry and Physics Discussions

Size-resolved measurement of the mixing state of soot in the megacity Beijing, China: diurnal cycle, aging and parameterization

Y. F. Cheng[1,2,7], H. Su[3], D. Rose[3], S. S. Gunthe[3,*], M. Berghof[2], B. Wehner[2], P. Achtert[2], A. Nowak[2], N. Takegawa[4], Y. Kondo[5], M. Shiraiwa[3], Y. G. Gong[6], M. Shao[1], M. Hu[1], T. Zhu[1], Y. H. Zhang[1], A. Wiedensohler[2], M. O. Andreae[3], and U. Pöschl[3]

[1]College of Environmental Sciences and Engineering, Peking University, Beijing 100871, China
[2]Leibniz Institute for Tropospheric Research, Leipzig, Germany
[3]Biogeochemistry Department, Max Planck Institute for Chemistry, Mainz 55020, Germany
[4]Research Center for Advanced Science and Technology, the University of Tokyo, Tokyo, Japan
[5]Department of Earth and Planetary Science, Graduate School of Science, the University of Tokyo, Tokyo 1130033, Japan

[6] Research Institute of Chemical Defence, Beijing 102205, China
[7] Center for Global and Regional Environment Research, University of Iowa, IA 52242, USA
[*] now at: EWRE Division, Department of Civil Engineering, Indian Institute of Technology Madras, Chennai 600036, India

Received: 4 November 2011 – Accepted: 22 November 2011 – Published: 7 December 2011

Correspondence to: H. Su (h.su@mpic.de)

Published by Copernicus Publications on behalf of the European Geosciences Union.

ACPD
11, 32161–32204, 2011

Abstract

Soot particles are regarded as the most efficient light absorbing aerosol species in the atmosphere, playing an important role as a driver of global warming. Their climate effects strongly depend on their mixing state, which significantly changes their light absorbing capability and cloud condensation nuclei (CCN) activity. Therefore, knowledge about the mixing state of soot and its aging mechanism becomes an important topic in the atmospheric sciences.

The size-resolved (30–320 nm diameter) mixing state of soot particles in polluted megacity air was measured at a suburban site (Yufa) during the CAREBeijing 2006 campaign in Beijing, using a Volatility Tandem Differential Mobility Analyzer (VTDMA). Particles in this size range with non-volatile residuals at 300 °C were considered to be soot particles. On average, the number fraction of internally mixed soot in total soot particles (F_{in}), decreased from 0.80 to 0.57 when initial D_p increased from 30 nm to 320 nm. Further analysis reveals that: (1) F_{in} was well correlated with the aerosol hygroscopic mixing state measured by a CCN counter. More externally mixed soot particles were observed when particles showed more heterogeneous features with regard to hygroscopicity. (2) F_{in} had pronounced diurnal cycles. For particles in the accumulation mode (D_p at 100–320 nm), largest F_{in} were observed at noon time, with "apparent" turnover rates ($k_{ex\rightarrow in}$) up to 7.8 % h^{-1}. (3) F_{in} was subject to competing effects of both aging and emissions. While aging increases F_{in} by converting externally mixed soot particles into internally mixed ones, emissions tend to reduce F_{in} by emitting more fresh and externally mixed soot particles. Similar competing effects were also found with air mass age indicators. (4) Under the estimated emission intensities, actual turnover rates of soot ($k_{ex\rightarrow in}$) up to 20 % h^{-1} were derived, which showed a pronounced diurnal cycle peaking around noon time. This result confirms that (soot) particles are undergoing fast aging/coating with the existing high levels of condensable vapors in the megacity Beijing. (5) Diurnal cycles of F_{in} were different between Aitken and accumulation mode particles, which could be explained by the faster size shift of smaller particles in the Aitken mode.

ACPD
11, 32161–32204, 2011

To improve the F_{in} prediction in regional/global models, we suggest parameterizing F_{in} by an air mass aging indicator, i.e., $F_{in} = a + bx$, where a and b are empirical coefficients determined from observations, and x is the value of an air mass age indicator. At the Yufa site in the North China Plain, fitted coefficients (a, b) were determined as (0.57, 0.21), (0.47, 0.21), and (0.52, 0.0088) for x (indicators) as $[NO_z]/[NO_y]$, [E]/[X] ([ethylbenzene]/[m,p-xylene]) and ([IM] + [OM])/[EC] ([inorganic + organic matter]/[elemental carbon]), respectively. Such a parameterization consumes little additional computing time, but yields a more realistic description of F_{in}.

1 Introduction

Soot particles are generally regarded as the most efficient light absorbing component of atmospheric aerosols (Hansen et al., 1979; Japar et al., 1986; Horvath, 1993; Bergstrom et al., 2007). They are produced by incomplete combustion of fossil fuel and biomass and they consist mainly of black or elemental carbon but may also contain some refractory organic matter (Horvath, 1993; Smith and O'Dowd, 1996; Burtscher et al., 2001; Novakov et al., 2003; Pöschl, 2005; Sadezky et al., 2005; Andreae and Gelencsér, 2006; Kondo et al., 2006, 2010; Rose et al., 2006; Frey et al., 2008; Cheng et al., 2009; Wehner et al., 2009). In the atmospheric science literature, the terms black carbon (BC), elemental carbon (EC), pyrogenic carbon are frequently used as synonyms for soot (e.g., Kondo et al., 2006, 2009; Pöschl et al., 2010). More discussion on this topic can be found in Andreae and Gelencsér (2006).

Soot particles, after emission, are generally undergoing aging processes by condensation (Smith et al., 1989), coagulation (Riemer et al., 2004, and references therein), as well as oxidation (Ivleva et al., 2007) and cloud/fog processing; and gradually become internally mixed (coated) with other chemical compounds. Depending on their mixing state, soot particles can be classified as internally mixed (coated) or externally mixed (uncoated). The mixing state of soot particles has a great influence on their climate effects. The light absorbing capability of soot (related to their direct radiative

ACPD
11, 32161–32204, 2011

effects) can be enhanced by a factor of 1.5 to 3 when soot is coated by or internally mixed with other aerosol components including sulfate, nitrate, organics and water (Jacobson, 2000; Lesins et al., 2002; Bond et al., 2006; Cheng et al., 2006, 2008a,b, 2009; Shiraiwa et al., 2008, 2010). Moreover, the coating of soot particles can significantly enhance their ability to be activated as cloud condensation nuclei (CCN) (Rose et al., 2011) and hence influence the cloud formation processes (related to their indirect radiative effects) and the removal of soot particles from the atmosphere. For these reasons, the mixing state is a crucial parameter for soot particles, uncertainty about which has been made difficult the accurate assessment of soot's climatic impact (Jacobson, 2001).

In global/regional climate models, the turnover rate ($k_{ex\rightarrow in}$) is used to describe the conversion rate of externally mixed to internally mixed soot particles. Due to limited knowledge and computational limits, a constant $k_{ex\rightarrow in}$ was taken in most studies, varying from 1.25 % h^{-1} to 2.5 % h^{-1} (Cooke and Wilson, 1996; Cooke et al., 1999, 2002; Lohmann et al., 2000; Jacobson, 2001; Koch, 2001). To obtain a more realistic $k_{ex\rightarrow in}$, several aerosol modeling studies have been carried out to examine quantitatively $k_{ex\rightarrow in}$ of soot particles (Riemer et al., 2004, 2010). However, it is challenging to validate the modeling results against atmospheric conditions, since modeling of the soot mixing state is almost equivalent to modeling all physicochemical processes in the gas and aerosol phases.

Decades ago, information about the soot mixing state relied on particle morphology measurements by Transmission Electron Microscopy (Katrinak et al., 1992, 1993; Hasegawa and Ohta, 2002). This technique does not always give reliable information, as volatile coatings may be lost, or thin coatings may not be evident. Later on, several online instruments with high time resolution were developed, i.e., volatility tandem differential mobility analyzer (VTDMA) (Philippin et al., 2004), single particle soot photometer (SP2) (Stephens et al., 2003) and aerosol time-of-flight mass spectrometer (ATOFMS) (Moffet and Prather, 2009). Among these methods, only the VTDMA is able to determine particle smaller than 0.1 µm. Based on these online methods, several

ACPD
11, 32161–32204, 2011

field studies have been carried out in recent years at regional (Engler et al., 2007), suburban (Shiraiwa et al., 2007; Cheng et al., 2009; Wehner et al., 2009), and urban sites (Rose et al., 2006), and by aircraft measurements (Moteki et al., 2007). The aging of soot particles was found to be well correlated with several air mass age indicators, e.g., ratios of C_2H_4 to C_2H_2 (Moteki et al., 2007), 2-pentyl nitrate (2-PeONO$_2$) to *n*-pentane (*n*-C_5H_{12}) (Shiraiwa et al., 2007) and OC/EC (organic carbon/elemental carbon) (Cheng et al., 2006). Under certain assumptions on the air mass history and OH concentrations, increase rates of F_{in} (number fraction of internally mixed soot particles) of about 1 % h^{-1} to 2.3 % h^{-1} were derived (Moteki et al., 2007; Shiraiwa et al., 2007).

In the summer of 2006, measurements of the mixing state of non-volatile particles (here taken to be "soot particles", see discussion in Sect. 2.2) were carried out at a suburban site of Beijing in the North China Plain by using a VTDMA (Cheng et al., 2009; Wehner et al., 2009). In this study, we perform an in-depth analysis of VTDMA results, focusing on the following topics: (1) comparison of the mixing state of soot measured by a VTDMA and the aerosol hygroscopicity mixing state determined by a CCN (cloud condensation nuclei) counter; (2) diurnal variation and evolution of soot mixing state at different size ranges; (3) calculation of $k_{ex\rightarrow in}$ and the influence on it of emissions; and (4) potential parameterization methods.

2 Methods

2.1 Overview of the campaign

As part of the "Campaign of Air Quality Research in Beijing and Surrounding Region 2006" (CAREBeijing 2006), air pollutants including aerosol and gases were comprehensively measured at a suburban site, Yufa (39.51467° N, 116.30533° E, ~25 m above ground level), during the summer of 2006. The Yufa site is located in the south of Beijing, roughly 50 km away from the urban center. One major road passes east of the

ACPD
11, 32161–32204, 2011

measurement site, at a distance of less than 200 m. Figure S1 (in the Supplement) shows the meteorological conditions at the Yufa site from 15 August to 9 September. During this period, the averages (± one standard deviation) of temperature, relative humidity (RH) and wind speed were 26.2 ± 3.7 °C, 68 ± 17 % and 1.6 ± 1.4 m s^{-1}, respectively (based on 5-min resolution meteorological data, see Supplement Fig. S1).

2.2 VTDMA measurement

A Volatility Tandem Differential Mobility Analyzer (VTDMA) (Orsini et al., 1996; Philippin et al., 2004) was used to measure the number size distributions of the non-volatile residuals of pre-selected mono-disperse particles that were heated at 300 °C (7 selected particle diameters in the range of 30 nm to 320 nm; time resolution of 1 h for a complete cycle of 7 diameters). In the thermal chamber (i.e., at 300 °C) of the VTDMA, the coating materials undergo volatilization leaving behind the non-volatile cores. Details about the VTDMA measurements at the Yufa site in 2006 can be found in Cheng et al. (2009) and Wehner et al. (2009). The volatilization results in a change of particle size, where unchanged particles indicate no coating material while big changes indicate a large fraction of coating materials. In continental polluted megacity air, the material of sub-micrometer particles that is non-volatile at this temperature (i.e., 300 °C) is considered to be mostly "soot" (Smith and O'Dowd, 1996; Burtscher et al., 2001; Kondo et al., 2006, 2010; Rose et al., 2006; Frey et al., 2008; Cheng et al., 2009; Wehner et al., 2009), which consists mainly of black or elemental carbon but may also contain some refractory organic matter (Pöschl, 2005; Sadezky et al., 2005; Andreae and Gelencsér, 2006). Since the VTDMA actually measures non-volatile-core containing particles (NVP), the notation "soot (NVP)" was mostly used instead of "soot" when referring to the VTDMA results.

In VTDMA measurements, the size distribution of nonvolatile residuals is classified into three groups according to $D_{p,300\,°C}/D_p$, where D_p is the initial diameter of the sampled dry particles and $D_{p,300\,°C}$ is the diameter of the particle residual after being heated at 300 °C. Following Wehner et al. (2009), (1) particles with $D_{p,300\,°C}/D_p < 45\,\%$

ACPD
11, 32161–32204, 2011

were denoted as "high-volatile" and not considered as soot particles; (2) particles with $45\,\% < D_{p,300\,^\circ C}/D_p < 82\,\%$ were denoted as "medium-volatile" and considered as internally mixed (coated) soot particles; and (3) Particles with $82\,\% < D_{p,300\,^\circ C}/D_p$ were denoted as "low-volatile" and considered as externally mixed (uncoated) soot particles.

F_{in}, the number fraction of internally mixed soot particles (among all soot-containing particles), was intensively used for discussion in this paper and calculated as,

$$F_{in} = n_{in}/(n_{in} + n_{ex}) \quad (1)$$

where n_{in} is the number concentration of internally mixed soot (NVP) particles, and n_{ex} is the number concentration of externally mixed soot (NVP) particles.

2.3 The turnover rate of soot particles

The turnover rate, $k_{ex\to in}$, is a parameter describing the conversion rate of the externally mixed soot to internally mixed particles:

$$\left(\frac{\partial n_{ex}}{\partial t}\right)_{ex\to in} = \left(\frac{\partial n_{ex}}{\partial t}\right)_{cond} + \left(\frac{\partial n_{ex}}{\partial t}\right)_{coag} = -k_{ex\to in} n_{ex} + \left(\frac{\partial n_{ex}}{\partial t}\right)_{coag} \quad (2)$$

where $\left(\partial n_{ex}/\partial t\right)_{ex\to in}$ is the rate of change of n_{ex} due to aging (conversion) processes. The two major aging processes are the condensation of sulfuric acid and organic compounds and the coagulation of particles. For large particles or during daytime, the condensation dominates the aging processes (Jacobson, 1997; Riemer et al., 2004), which converted equal amounts of externally mixed soot to internally mixed. Then the rate of change of n_{in} due to aging (conversion) processes is

$$\left(\frac{\partial n_{in}}{\partial t}\right)_{ex\to in} \approx -\left(\frac{\partial n_{ex}}{\partial t}\right)_{ex\to in} = k_{ex\to in} n_{ex} \quad (3)$$

The values of n_{ex} and n_{in} measured in field campaigns can be subject to other processes, e.g., horizontal/vertical transport ($Tran_{ex}$ and $Tran_{in}$), emission ($Emis_{ex}$ and

ACPD
11, 32161–32204, 2011

$\mathrm{Emis_{in}}$), and deposition ($\mathrm{Depo_{ex}}$ an $\mathrm{Depo_{in}}$):

$$\frac{\partial n_{\mathrm{ex}}}{\partial t} = \mathrm{Tran_{ex}} + \mathrm{Emis_{ex}} + \mathrm{Depo_{ex}} + \left(\frac{\partial n_{\mathrm{ex}}}{\partial t}\right)_{\mathrm{ex}\to\mathrm{in}} \tag{4}$$

$$\frac{\partial n_{\mathrm{in}}}{\partial t} = \mathrm{Tran_{in}} + \mathrm{Emis_{in}} + \mathrm{Depo_{in}} + \left(\frac{\partial n_{\mathrm{in}}}{\partial t}\right)_{\mathrm{ex}\to\mathrm{in}} \tag{5}$$

When aging is the only or dominant process affecting n_{ex} and n_{in},

$$\frac{\partial n_{\mathrm{ex}}}{\partial t} \approx \left(\frac{\partial n_{\mathrm{ex}}}{\partial t}\right)_{\mathrm{ex}\to\mathrm{in}} = -k_{\mathrm{ex}\to\mathrm{in}} n_{\mathrm{ex}} \tag{6}$$

$$\frac{\partial n_{\mathrm{in}}}{\partial t} \approx \left(\frac{\partial n_{\mathrm{in}}}{\partial t}\right)_{\mathrm{ex}\to\mathrm{in}} = k_{\mathrm{ex}\to\mathrm{in}} n_{\mathrm{ex}} \tag{7}$$

$$\left(\frac{\partial n_{\mathrm{tot}}}{\partial t}\right)_{\mathrm{ex}\to\mathrm{in}} = \left(\frac{\partial n_{\mathrm{ex}}}{\partial t}\right)_{\mathrm{ex}\to\mathrm{in}} + \left(\frac{\partial n_{\mathrm{in}}}{\partial t}\right)_{\mathrm{ex}\to\mathrm{in}} = 0 \tag{8}$$

where $\partial n_{\mathrm{tot}}/\partial t$ is the rate of change of total (ex + in) soot particles. $(\partial n_{\mathrm{tot}}/\partial t)_{\mathrm{ex}\to\mathrm{in}} = 0$ indicates that $n_{\mathrm{tot}}$is constant in the aging (ex → in) process dominated by the condensation.

In aging processes, the rate of change of F_{in} ($F_{\mathrm{in}} = n_{\mathrm{in}}/n_{\mathrm{tot}}$) is

$$\left(\frac{\partial \frac{n_{\mathrm{in}}}{n_{\mathrm{tot}}}}{\partial t}\right)_{\mathrm{ex}\to\mathrm{in}} = k_{\mathrm{ex}\to\mathrm{in}} \frac{n_{\mathrm{ex}}}{n_{\mathrm{tot}}} \tag{9}$$

$$\left(\frac{\partial F_{\mathrm{in}}}{\partial t}\right)_{\mathrm{ex}\to\mathrm{in}} = k_{\mathrm{ex}\to\mathrm{in}}(1 - F_{\mathrm{in}}) \tag{10}$$

Then the turnover rate $k_{\mathrm{ex}\to\mathrm{in}}$ can be calculated by

$$k_{\mathrm{ex}\to\mathrm{in}} = \frac{\left(\partial F_{\mathrm{in}}/\partial t\right)_{\mathrm{ex}\to\mathrm{in}}}{(1 - F_{\mathrm{in}})} \approx \frac{\left(\partial F_{\mathrm{in}}/\partial t\right)}{(1 - F_{\mathrm{in}})} \approx \frac{\left(\Delta F_{\mathrm{in}}/\Delta t\right)}{(1 - F_{\mathrm{in}})} \tag{11}$$

ACPD
11, 32161–32204, 2011

When aging (ex → in) dominates the variation of F_{in}, $k_{ex \rightarrow in}$ can be determined by Eq. (11). When other processes become significant, this conclusion will not hold and $k_{ex \rightarrow in}$ determined by Eq. (11) is called the "apparent" turnover rate. Increase rates ($\Delta F_{in}/\Delta t$) of 1.0–2.3 % h^{-1} and F_{in} of 0.2–0.6 were reported in previous studies (Moteki et al., 2007; Shiraiwa et al., 2007), corresponding to "apparent" $k_{ex \rightarrow in}$ of 1.3–5.8 % h^{-1}.

2.4 CCN measurement and hygroscopicity (κ) distribution

Size-resolved CCN efficiency spectra (activation curves) were measured with a Droplet Measurement Technologies continuous flow CCN counter (DMT-CCNC) coupled to a Differential Mobility Analyzer (DMA; TSI 3071) and a Condensation Particle Counter (CPC; TSI 3762). The CCNC was operated at a total flow rate of 0.5 l min^{-1} with a sheath-to-aerosol flow ratio of 10. The effective water vapor supersaturation (S) was regulated by the temperature difference between the upper and lower end of the CCNC flow column (ΔT) and calibrated with ammonium sulfate aerosol as described by Rose et al. (2008). For a detailed description of CCN measurements in the campaign, see Gunthe et al. (2011).

Size-resolved CCN efficiency spectra can be used to derive the cumulative distribution function of particle hygroscopicity, $H(\kappa, D_p)$, which is defined as the number fraction of particles with a given dry diameter, D_p, and with an effective hygroscopicity parameter smaller than the parameter κ (Su et al., 2010). The data conversion from S-D_p space to κ-D_p space is achieved by solving the κ-Köhler model equation (Petters and Kreidenweis, 2007).

By fitting $H(\kappa, D_p)$ with a cumulative single-mode lognormal distribution function (CDF), the following parameters were calculated: $\overline{\kappa}_g$, the geometric mean of κ in the fitted mode; and $\sigma_{\kappa,g}$, the geometric standard deviation of κ in the fitted mode. The spread of the κ distribution, e.g., $\sigma_{\kappa,g}$, reflects the mixing state of aerosols: under internally mixed conditions, all particles have the same composition and a uniform hygroscopicity mode, while under externally mixed conditions, particles can have distinct hygroscopicity modes (see Fig. 1).

ACPD
11, 32161–32204, 2011

2.5 Air mass age indicator

The aging of soot particles results in a change of their mixing state, i.e., conversion of externally mixed to internally mixed soot. An aged air mass has a larger fraction of internally mixed soot than a fresh air mass. Therefore, correlations can be expected between an air mass age indicator and the soot mixing state parameter (e.g., F_{in}). If such a correlation is significant, the soot mixing state could be parameterized by the air mass age indicators.

The age of air mass is a concept under the Lagrangian system. Ideally, the most fresh air mass is assigned an age of zero and its age will increase as the air mass becomes aged. The longer the air mass travels in the atmosphere, the older it will be. However, this does not mean that the age of an air mass can become infinitely large, and injection of fresh emissions into the air mass would reduce its age.

To quantify air mass ages, several indicators have been proposed. They are based on the fact that the aging will change the chemical compositions of air masses and parameters reflecting such changes can indicate the aging stage. Three indicators were used in this study.

$[NO_z]/[NO_y]$

In a fresh air mass from combustion sources, NO_x (NO_x=NO + NO_2) are the dominant components of NO_y (the total odd nitrogen compounds in the atmosphere). As photochemical reactions proceed, NO_x evolves to other N-containing compounds such as HNO_3 and PAN, and the ratio of $[NO_z]/[NO_y]$ (NO_z=NO_y−NO_x) will increase. In this study, the nitrogen oxides (NO_x) and total reactive nitrogen (NO_y) were measured using a NO-O_3 chemiluminescence detector combined with a photolytic converter and a gold tube catalytic converter (Takegawa et al., 2006)

[E]/[X]

The ratios of hydrocarbons have been used as measures of photochemical age since Calvert (1976). Different reactivities of hydrocarbons result in different removal rates

ACPD
11, 32161–32204, 2011

and monotonic change of their ratios in the aging process. We used the ratio of ethylbenzene and m,p-xylene ([E]/[X]) in this study. Ethylbenzene and m,p-xylene were measured by an online GC-PID (gas chromatograph-photo ionization detector) system, as detailed by Xie et al. (2008).

$$([IM]+[OM])/[EC]$$

As an air mass ages, more secondary aerosol is produced, which reduce the mass fraction of soot particles. $([IM]+[OM])/([EC])$ could hence be used as an indicator, in which $[IM]=[NH_4^+]+[NO_3^-]+[SO_4^{2-}]+[Cl^-]$ (inorganic ions in PM_1 measured by aerosol mass spectrometer, AMS) and [OM] was the organic matter mass (in PM_1) determined by AMS. An online Sunset EC/OC analyzer was used to measure the mass concentrations of EC, [EC]. Details about the EC/OC analyzer and AMS can be found in Takegawa et al. (2009).

3 Results and discussion

3.1 The mixing state of soot and hygroscopicity

Table 1 summarizes statistics of F_{in} measurements from this campaign. The F_{in} values show a decreasing trend as the particle size D_p increases, ranging from an $\overline{F_{in}}$ of 0.80 ± 0.075 at $D_p = 30$ nm to $\overline{F_{in}}$ of 0.57 ± 0.102 at $D_p = 320$ nm (arithmetic mean $\pm$ standard deviation). Figure 2 shows a comparison of hourly F_{in} data with $\sigma_{\kappa,g}$ (the geometric standard deviation in a lognormal κ distribution, as detailed in Sect. 2.4., and Su et al., 2010). The $(1-F_{in})$ is the number fraction of externally mixed soot (NVP) particles. The two parameters, $\sigma_{\kappa,g}$ and $(1-F_{in})$, are well correlated. This means that more externally mixed soot (NVP) particles were observed when particles showed more heterogeneous features in their hygroscopicity distributions (large $\sigma_{\kappa,g}$). Such consistence gives confidence about the robustness of both parameters and the reliability of the measuring systems.

ACPD
11, 32161–32204, 2011

3.2 Diurnal cycle of the soot mixing state

Figure 3 shows a pronounced diurnal cycle of F_{in}, which also has a strong size dependence. For accumulation mode particles (i.e., 100 nm to 320 nm, Fig. 3b), similar diurnal profiles of F_{in} can be found, with a maximum at ~13:00 LT (local time) and two minimums, in the early morning ~7:00 LT and at night ~21:00 LT, respectively. As the day progresses, an increase in F_{in} (8:00–13:00 LT) is observed for accumulation mode particles with "apparent" turnover rates of 6.7–7.8 % h^{-1}.

In the Aitken mode, however, the variation of F_{in} is different to that in the accumulation mode (Fig. 3a). The maximum of F_{in} appears earlier at ~8:00 LT (at D_p = 30 nm) and 12:00 LT (at D_p = 50 nm), and the afternoon minimum F_{in} appears earlier as well. The distinct behaviors of Aitken mode particles are shown by the correlation matrix in Table 2, where F_{in} of Aitken mode particles show poor correlations with the accumulation mode particles. The reasons for such correlations will be further discussed in Sect. 3.5.

For accumulation mode particles presented in Fig. 3b, F_{in} shows a peak around noon time. Such a diurnal cycle indicates that ground-based measurements were subject to competing effects from physico-chemical aging and the introduction of fresh emissions. While the aging increases F_{in} by turning externally mixed particles into internally mixed ones, the fresh emissions, with low F_{in}, tend to reduce the F_{in} values. Similar competing effects can also be found in the diurnal courses of the air mass age indicators (e.g., $[NO_z]/[NO_y]$, [E]/[X] and ([IM]+[OM])/[EC] in Fig. 4) and aerosol single scattering albedo as reported in Garland et al. (2008).

3.3 Estimation of soot emission rate

Emissions have a significant impact on the measured F_{in} and the "apparent" $k_{ex \to in}$ (soot turnover rate). Before determining the actual $k_{ex \to in}$, we need to first quantify the emissions.

ACPD
11, 32161–32204, 2011

Figure 5 shows the diurnal cycles of three parameters: (1) normalized EC concentrations during the campaign, (2) normalized total (ex + in) soot emission rates, and (3) the ratio of normalized emission rate to EC concentrations. The EC concentrations were determined by an online Sunset EC/OC analyzer (Takegawa et al., 2009); and the (total) soot emission rate was supposed to be proportional to the CO emissions in Beijing (Zhou et al., 2010). The normalized parameters were defined as the ratio of the individual parameter to its daily average value. For example, given [EC] of 9 μg cm^{-3} at 9:00 LT and a daily mean ($\overline{[EC]}$) of 10 μg cm^{-3}, the normalized EC concentration ([EC]*) at 9:00 LT is then 0.9 (i.e., 0.9 = 9 μg cm^{-3}/10 μg cm^{-3}).

The sum of Eqs. (4) and (5) gives the total (ex + in) emissions of soot particles

$$\mathrm{Emis_{tot}} = \frac{\Delta n_{\mathrm{tot}}}{\Delta t} - \mathrm{Tran_{tot}} - \mathrm{Depo_{tot}} \text{ and } \mathrm{Emis_{tot,m}} = \frac{\Delta m_{\mathrm{tot}}}{\Delta t} - \mathrm{Tran_{tot,m}} - \mathrm{Depo_{tot,m}} \quad (12)$$

where $\mathrm{Emis_{tot,m}}$ is the mass emission rate of soot, and m_{tot} is the mass concentration of soot.

To obtain an optimal estimate of $\mathrm{Emis_{tot}}$ (or $\mathrm{Emis_{tot,m}}$), we adopted the following criteria, eliminating days with average wind speed > 2 m s^{-1} (20, 22 August, 3, 4, 5, 6 and 8 September), excluding the time periods from 8:00 to 19:00 LT, and choosing periods with large $\mathrm{Emis_{tot,m}}/m_{\mathrm{tot}}$. The goal is to minimize the impact of horizontal/vertical transport and deposition, and choosing low wind speeds and night-time periods avoid large influence of horizontal transport and vertical mixing. Large $\mathrm{Emis_{tot,m}}/m_{\mathrm{tot}}$ ensures that the emission term could dominate the variation of m_{tot}.

In practice, we first calculated the diurnal variation of the three parameters (normalized $m^*_{\mathrm{tot}} = [\mathrm{EC}]^*$, $\mathrm{Emis^*_{tot,m}}$, and $\mathrm{Emis^*_{tot,m}}/m^*_{\mathrm{tot}}$) on days with average wind speed < 2 m s^{-1}. Then we looked for the highest ratios of $\mathrm{Emis^*_{tot,m}}/m^*_{\mathrm{tot}}$ (labeled as "emission/concentration" in Fig. 5) in the period of 20:00–7:00 LT. In the end, the optimal emission rate was determined by $\mathrm{Emis_{tot,m}} = \Delta[\mathrm{EC}]/\Delta t$ at 20:00 LT, when the selected $\mathrm{Emis^*_{tot,m}}/m^*_{\mathrm{tot}}$ data reached its maximum. The ratio of the mean (mass) emission rate to mean (mass) concentration, $\overline{\mathrm{Emis_{tot,m}}}/\overline{[\mathrm{EC}]}$, can then be determined by

ACPD
11, 32161–32204, 2011

$$\frac{\overline{\mathrm{Emis}_{\mathrm{tot,m}}}}{\overline{[\mathrm{EC}]}} = \frac{\mathrm{Emis}_{\mathrm{tot,m}}}{[\mathrm{EC}]} \times \frac{[\mathrm{EC}]^*}{\mathrm{Emis}^*_{\mathrm{tot,m}}} \approx \frac{\Delta[\mathrm{EC}]/\Delta t}{[\mathrm{EC}]} \times \frac{[\mathrm{EC}]^*}{\mathrm{Emis}^*_{\mathrm{tot,m}}} \text{ at 20:00 LT} \approx 13\,\%\ \mathrm{h}^{-1} \quad (13)$$

In the following analysis, we took the same value ($13\,\%\,\mathrm{h}^{-1}$) for the estimated ratio of the mean (number) emission rate to mean (number) concentration, $\overline{\mathrm{Emis}_{\mathrm{tot}}}/\overline{n_{\mathrm{tot}}}$.

3.4 Actual turnover rate of soot

In this section, a conceptual model was used to analyze the observed variation of F_{in}. Since F_{in} of particles of all sizes in the accumulation mode (i.e., 100–320 nm) showed similar behaviors, F_{in} at 150 nm is taken as an example and will be discussed through this section.

Two processes were considered in the model: the aging process converting externally mixed particles into internally mixed particles, and the addition of fresh emissions. Equations (4) and (5) can be simplified as:

$$\frac{\Delta n_{\mathrm{in}}}{\Delta t} = \left(\frac{\partial n_{\mathrm{in}}}{\partial t}\right)_{\mathrm{ex}\to\mathrm{in}} + \mathrm{Emis}_{\mathrm{in}} = k_{\mathrm{ex}\to\mathrm{in}} n_{\mathrm{ex}} + \mathrm{Emis}_{\mathrm{in}} \quad (14)$$

$$\frac{\Delta n_{\mathrm{ex}}}{\Delta t} = -k_{\mathrm{ex}\to\mathrm{in}} n_{\mathrm{ex}} + \mathrm{Emis}_{\mathrm{ex}} \text{ and } \frac{\Delta n_{\mathrm{tot}}}{\Delta t} = \mathrm{Emis}_{\mathrm{tot}} \quad (15)$$

where $k_{\mathrm{ex}\to\mathrm{in}}$ denotes the turnover rate of externally mixed into internally mixed soot, n_{tot} is the number concentration of all soot particles (including both internally and externally mixed ones), $\mathrm{Emis}_{\mathrm{in}}$, $\mathrm{Emis}_{\mathrm{ex}}$, and $\mathrm{Emis}_{\mathrm{tot}}$ are the emission rates of internally mixed, externally mixed, and total soot particles, respectively.

In Eqs. (14) and (15), we assumed that all (or most) particles stayed in the same size bin after the 1-h aging process. This assumption, to a large extent, simplified the following analysis, and could at least be valid for a broader size bracket, e.g., [100 nm, 350 nm]. The transport and dry deposition processes were supposed not to significantly change F_{in} (assuming n_{in} and n_{ex} have the same gradient and dry deposition velocity) and were therefore ignored in this analysis.

ACPD
11, 32161–32204, 2011

The variation of F_{in} in the time interval Δt can be derived by combining Eqs. (14) and (15):

$$\Delta F_{in} = \frac{n_{in} + \Delta n_{in}}{n_{tot} + \Delta n_{tot}} - F_{in} = \frac{n_{in} + (k_{ex\to in}(n_{tot} - n_{in}) + \mathrm{Emis}_{in})\Delta t}{n_{tot} + \mathrm{Emis}_{tot}\Delta t} - F_{in} \quad (16)$$

Then $k_{ex\to in}$ can be expressed as a function of n_{tot}, F_{in}, Emis_{tot} and Emis_{in},

$$k_{ex\to in} = \frac{(\Delta F_{in} + F_{in})(1 + \frac{\mathrm{Emis}_{tot}\Delta t}{n_{tot}}) - F_{in} - \frac{\mathrm{Emis}_{in}\Delta t}{n_{tot}}}{(1 - F_{in})\Delta t} \quad (17)$$

where, n_{tot} and F_{in} can be determined by VTDMA measurements. Emis_{tot} can be calculated by multiplying a generic diurnal cycle of emissions in Beijing (Fig. 5) by the estimated emission intensity ($\overline{\mathrm{Emis}_{tot}}/\overline{n_{tot}}$) of 13 % h^{-1} (details in Sect. 3.3). Emis_{in} can be calculated by multiplying Emis_{tot} with an emission factor, $\beta = \mathrm{Emis}_{in}/\mathrm{Emis}_{tot}$. The minimum $F_{in} \sim 0.6$ can be considered as the upper limit of β, and we also chose several other β values (0.2 and 0.4) for sensitivity studies.

Figure 6 shows the diurnal cycles of campaign-averaged $k_{ex\to in}$ calculated for particles at 150 nm with different β. Compared to a fixed $k_{ex\to in}$ value commonly used in regional and global models, the observation-constrained $k_{ex\to in}$ shows higher values with a maximum around 11:00–15:00 LT, and low values in the early morning and late afternoon. Such a diurnal course always holds, even after varying Emis_{tot} by a factor of two (6.5–26 % h^{-1}). The cycle of the turnover rate, $k_{ex\to in}$, supports previous results in modeling studies (Riemer et al., 2004, 2010), which show high daytime $k_{ex\to in}$ dominated by condensation processes, and low $k_{ex\to in}$ contributed by both slower condensation and coagulation processes in the early morning and late afternoon. Although $k_{ex\to in}$ were also calculated for night-time periods, attention should be paid to these values. Because the coagulation-induced aging would become more important than the condensation, which violates the assumption of our model calculations.

Since the condensation-induced turnover rate is proportional to the condensable vapor pressure, the derived daytime $k_{ex\to in}$ implies a peak of condensable vapor pressure

ACPD
11, 32161–32204, 2011

at the same period (11:00–15:00 LT). It is already known that gaseous sulfuric acid (precursor of sulfate in particles) often shows a peak around noon time. Our results indicate that even the potentially present un-identified condensable vapors might have similar diurnal cycles as sulfuric acid. Instead of complete characterizations of these un-identified vapors, the similarity in their diurnal variations enables the use of a simple parameterization method as an alternative solution in aerosol modeling studies, as will be discussed below.

Due to the presence of primary emission sources, the actual turnover rate of soot, $k_{ex\rightarrow in}$ is higher than the "apparent" $k_{ex\rightarrow in}$. The freshly emitted particles contain more externally mixed soot than the aged ambient air. The observed "aging" of soot (NVP) is to a certain extent compensated by the fresh emissions, the extent of which depends on the emission intensity. For the estimated emission intensity ($\overline{\mathrm{Emis}_{tot}}/\overline{n_{tot}}$) of 13 % h^{-1} and $\beta = 0.6$, $k_{ex\rightarrow in}$ values reached up to 20 % h^{-1} (see Fig. 6), much faster than the apparent $k_{ex\rightarrow in}$ of 6.7–7.8 % h^{-1}.

The aging process in Beijing is also much faster than $k_{ex\rightarrow in}$ of 1.3–5.8 % h^{-1} in previous field measurements (Moteki et al., 2007; Shiraiwa et al., 2007) and 1.25–2.5 % h^{-1} in modeling studies (Cooke and Wilson, 1996; Cooke et al., 1999, 2002; Lohmann et al., 2000; Jacobson, 2001; Koch, 2001; Tsigaridis and Kanakidou, 2003; Riemer et al., 2004). The fast turnover rate in the polluted megacity air is consistent with the observed rapid particle growth in the same area (Wiedensohler et al., 2009), both of which can be attributed to the fast formation and condensation of secondary aerosols in the megacity. The flow of soot particles from megacities influences the global background of soot to a large extent. If those soot particles are already coated or internally mixed in a very short time due to strong condensation, the background soot should be mostly internally mixed, as has been suggested by Andreae and Rosenfeld (2008).

Figure 6 also shows that the absolute value of $k_{ex\rightarrow in}$ strongly depends on the choice of the emission factor β, while the relative variation of $k_{ex\rightarrow in}$ does not. Smaller β values (large fraction of externally mixed soot in emissions) require faster $k_{ex\rightarrow in}$ to explain the

ACPD
11, 32161–32204, 2011

observed F_{in} variations. For example, $\beta = 0.2$ requires $k_{ex \to in}$ up to 70 % h^{-1} to meet the observations. On the other hand, $k_{ex \to in}$ up to 20 % h^{-1} require a large $\beta = 0.6$, which means that 60 % of the emitted soot particles should have already been internally mixed when they arrive at the measurement site.

3.5 Distinct diurnal variations of F_{in} for Aitken and accumulation mode particles

In the conceptual model, we assume that particle growth will not lead to significant change in n_{tot} and n_{ex}, which means no significant shift of the particle size distribution occurs over a short time. While such an assumption is valid for large particles in the accumulation mode (i.e., > 100 nm), it might be violated by the faster growth of small particles (e.g., 30 nm) in the Aitken mode, which was reflected by the different diurnal cycles of F_{in} at smaller diameters (see Fig. 3).

To describe the rate of change of a particle size distribution $n(D_p)$ resulting from condensation, we adopted a general condensation equation (Seinfeld and Pandis, 2006, pp. 591) in the form

$$\frac{\partial n}{n \partial t} = -\frac{\partial}{n \partial D_p}\left(n \frac{4DM}{RTD_p\rho_p} f(Kn,\alpha)P\right) \quad (18)$$

where n denotes the particle number concentration at D_p, M is the molecular weight for the condensable species, D is its diffusion coefficient in air, R is the molar gas constant, T is the temperature (in Kelvin), ρ_p is the density of the particles, P is the supersaturated vapor pressure of the condensable species, Kn is the Knudsen number ($Kn = 2\lambda/D_p$), λ is the mean free path of the condensable species in air, and α is the accommodation coefficient of the condensable species. $f(Kn, \alpha)$ is the correction due to non-continuum effects and imperfect surface accommodation and can be calculated by

$$f(Kn,\alpha) = \frac{0.75\alpha(1+Kn)}{Kn^2 + Kn + 0.283Kn\alpha + 0.75\alpha} \quad (19)$$

ACPD
11, 32161–32204, 2011

Dividing both sides of Eq. (18) by $A = 4DMP/(RT\rho_p)$, we get a parameter k_{shift}:

$$k_{shift} = \frac{1}{A}\frac{\partial n}{n\partial t} = -\frac{\partial}{n\partial D_p}\left(\frac{n}{D_p}f(Kn,\alpha)\right) \quad (20)$$

k_{shift} differs from $(\partial n/\partial t)/n$ in Eq. (18) by a factor of A, which is generally/mostly independent of particle sizes. So, k_{shift} is equivalent to $(\partial n/\partial t)/n$ in representing the size dependence of the rate of change of n due to condensation. By taking the measured $n(D_p)$ and $\lambda = \lambda_{air}$ (298 K, 1 atm) = 65.1 nm (Seinfeld and Pandis, 2006, p. 399), k_{shift} can be calculated for each D_p.

Figure 7 shows k_{shift} as a function of the particle size D_p, calculated with Eqs. (18)–(20) for the CAREBeijing 2006 campaign. The (mean) size distributions of the internally (externally) mixed soot (NVP) particles were used in the calculation (Wehner et al., 2009). Since VTDMA measurements covered only a limited size range (from 30 nm to 320 nm), nearest neighbor extrapolation were performed for out of range values, i.e. [1 nm, 30 nm) and (320 nm, 1000 nm] as shown in Fig. 7. k_{shift} shows positive values roughly on the right side of the peak of the particle size distributions and negative values on the left side. Positive k_{shift} (at D_p in shaded areas) indicate condensation-induced increases in $n(D_p)$ while negative k_{shift} (at D_p in un-shaded areas) indicate condensation-induced decreases in $n(D_p)$. Since the peaks of the $n_{in}(D_p)$ and $n_{ex}(D_p)$ distributions appears at sizes smaller than 100 nm, the condensation growth generally increases $n_{in}(D_p)$ in the accumulation mode and reduces $n_{in}(D_p)$ at the D_p of 30 nm.

Equation (21) describes the rate of change of internally mixed soot particles due to the condensational growth

$$\frac{\Delta n_{in}}{\Delta t} = A n_{in} k_{in,shift} \quad (21)$$

where $k_{in,shift}$ represent k_{shift} of internally mixed soot particles.

For externally mixed soot particles, the condensational growth results in a rate of change in the opposite direction of Eq. (21). Laboratory experiments showed that

ACPD
11, 32161–32204, 2011

(externally mixed) soot agglomerates after sulfuric acid exposure (condensation) exhibit a considerable restructuring and shrinking to a more compact form (Zhang et al., 2008). By assuming a shrink speed (of n_{ex}) similar to the growth speed (of n_{in}), the rate of change of externally mixed soot particles due to condensational growth can be expressed by Eq. (22), in which ε is the conversion coefficient of the growing to shrinking speed.

$$\frac{\Delta n_{ex}}{\Delta t} = -A\varepsilon n_{ex} k_{ex,shift} \quad (22)$$

$$\frac{\Delta n_{tot}}{\Delta t} = \frac{\Delta n_{in} + \Delta n_{ex}}{\Delta t} = A n_{in} k_{in,shift} - A\varepsilon n_{ex} k_{ex,shift} \quad (23)$$

According to Eqs. (22) and (23), the condensation-induced shift of size distributions tends to reduce F_{in} of Aitken mode particles (a decrease in n_{in} and an increase in n_{ex}) while the emissions begin to counteract (or buffer) the influence of condensation. In Fig. 3a, the variation of F_{in} at $D_p = 30$ nm is a good example of such competition: the condensation overwhelmed the emissions at 8:00–15:00 LT causing a decrease in F_{in}, while the emission became more important from 15:00 to 19:00 LT resulting in an increasing F_{in}. For particles at $D_p = 50$ nm, $k_{in,shift}$ is not as fast as that at 30 nm. So the emissions and $k_{ex\rightarrow in}$ needed to be considered along with $k_{in,shift}$, which results in an intermediate variation of F_{in}.

3.6 Size-resolved parameterizations of F_{in}

Because of our insufficient knowledge on mixing states and their change and the computational costs associated with explicit modeling of the mixing processes, it is still difficult to explicitly and accurately predict the variation of F_{in} in regional/climate models. In an aging air mass, the change of soot mixing state is generally accompanied by the change of other indicators representing the air mass age. We suggest parameterizing the mixing state of soot by using these correlations. If the other indicators

ACPD
11, 32161–32204, 2011

are easier to measure and model, such parameterizations might provide an alternative solution, narrowing down the differences between ambient and modeled soot mixing state without significant additional computational costs.

The proposed parameterization approach involves two steps to calculate F_{in} from other indicators. First, the average diurnal values of F_{in} and other parameters (as shown in Figs. 3 and 4) are adopted to calculate a linear fit, resulting in the parameterization Eqs. (24)–(26). The reason for using average values is to smooth out fluctuations which may greatly reduce the correlation coefficient R and introduce large uncertainties into the fitting results. F_{in} at certain diameter (i.e., 150 nm) can be predicted by parameterization Eqs. (24)–(26). Figure 8a–c shows comparisons of F_{in} at 150 nm with individual indicators, namely, $[NO_z]/[NO_y]$, [E]/[X] and ([IM] + [OM])/[EC].

$$F_{in}(150\,\text{nm}) = 0.572 + 0.209\frac{[NO_z]}{[NO_y]} \quad (24)$$

$$F_{in}(150\,\text{nm}) = 0.468 + 0.212\frac{[E]}{[X]} \quad (25)$$

$$F_{in}(150\,\text{nm}) = 0.522 + 0.0088\frac{[IM]+[OM]}{[EC]} \quad (26)$$

Secondly, the size-resolved F_{in} in the accumulation mode can be calculated by the following equation from F_{in} at 150 nm:

$$F_{in}(D_p) = (a\log 10(D_p/1\,\text{nm}) + b)F_{in}(150\,\text{nm}) \quad (27)$$

where a and b are constant parameters.

Fitting Eq. (27) to the measured F_{in} over the diameter range 100 nm to 320 nm, we got $a = -0.353$ (-0.370, -0.336) (coefficients with 95 % confidence bounds), $b = 1.78$ (1.74, 1.82), and $R^2 = 0.80$. Figure 9 and Table 3 shows that Eq. (27) performs well in predicting the size-resolved F_{in} over the size range between 100 nm and 320 nm. There is no systematic underestimation (or overestimation) and the fitted slope k is almost

ACPD
11, 32161–32204, 2011

the same as the 1 : 1 line. Most variations, i.e., up to 77 %, of F_{in} can be predicted by the parameterization.

4 Conclusions

Analysis of VTDMA results from the megacity Beijing shows a pronounced diurnal variation of F_{in} with different time courses in the Aitken and accumulation modes. For accumulation mode particles, maxima of F_{in} were observed at 12:00–13:00 LT, which can be explained by competing effects of physicochemical conversion and direct emissions. The distinct diurnal cycles of F_{in} of Aitken and accumulation mode particles are likely to be caused by faster growth of smaller Aitken mode particles.

To calculate the actual turnover rate of soot from external to internal mixture ($k_{ex\rightarrow in}$), measurement data were analyzed by a conceptual model, which considered both direct emissions and the aging process. The analysis shows that the actual $k_{ex\rightarrow in}$ has high values during daytime, i.e., a maximum around 11:00–15:00 LT, and low values during the night-time. Turnover rates reached values of 20–70 % h^{-1} around mid-day, which implies that soot (NVP) particles are present to a large extent as internal mixtures by the time the leave the urban environment. This enables them to act as CCN and also facilitates their removal by wet deposition (Andreae and Rosenfeld, 2008). The cycle of $k_{ex\rightarrow in}$ supports previous modeling results implying that the un-identified condensable vapors might have similar diurnal variations as sulfuric acid and other short life-time compounds produced by photochemistry. We also found that due to injection of fresh emissions, the "apparent" turnover rates derived from the variation in F_{in} were much smaller than the actual $k_{ex\rightarrow in}$.

In this study, the calculated $k_{ex\rightarrow in}$ might be subject to potential uncertainties due to: (1) the estimation of $Emis_{tot}$ (soot emission intensity) and β (number fraction of internally mixed soot particles in emissions); (2) the effect of transport process; and (3) the influence of particle growth and coagulation. To better understand the soot aging process, we suggest measuring β in some emission studies, combining regional

ACPD
11, 32161–32204, 2011

models to quantify the transport effects, and implementing aerosol dynamic models instead of the current conceptual model.

F_{in} shows a similar diurnal course as the other air mass age indicators (e.g., $[NO_z]/[NO_y]$, [E]/[X] and ([IM]+[OM])/[EC]), which are subject to competing effects between emissions and aging processes as well. The good agreement of their correlations can be expressed as a linear relationship. Given the difficulty of making direct measurements of soot mixing state (F_{in}), these relationships might be of great practical value in regional/global-scale studies on the influence of the various direct and indirect soot aerosol effects on climate, as it provides an easily measured proxy that does not consume significant additional computing time. However, such parameterizations require caveats because considerable variability can be expected between different sites or even at a given site, like the scattered data shown in Figs. 8 and 9. To validate the parameterization methods, improve our understanding and refine the range of the fitting parameters, more measurements should be carried out in other environments. In addition, validation for particles larger than 320 nm needs to be performed in future studies.

Appendix A

See Tables A1 and A2 for acronyms and symbols.

Supplementary material related to this article is available online at: http://www.atmos-chem-phys-discuss.net/11/32161/2011/acpd-11-32161-2011-supplement.pdf.

Acknowledgements. The CAREBeijing 2006 campaign was supported by the Beijing Council of Science and Technology (HB200504-6, HB200504-2). This study was supported by the Max Planck Society (MPG), the Leibniz Institute for Tropospheric Research (IfT), Peking University, and the University of Tokyo (UT). Hang Su's work was supported in part by MPG, the

ACPD
11, 32161–32204, 2011

Pan-European Gas-AeroSOls-climate interaction Study (No. 265148, PEGASOS) and the European integrated project on aerosol cloud climate and air quality interactions (No. 036833-2, EUCAARI). Y. Kondo and N. Takegawa were supported by the Ministry of Education, Culture, Sports, Science, and Technology (MEXT) and the global environment research fund of the Japanese Ministry of the Environment (A-0803 and A-1101). Thanks are owed to all the team members of CAREBeijing 2006 for support during the campaign.

References

Andreae, M. O. and Gelencsér, A.: Black carbon or brown carbon? The nature of light-absorbing carbonaceous aerosols, Atmos. Chem. Phys., 6, 3131–3148, doi:10.5194/acp-6-3131-2006, 2006.

Andreae, M. O. and Rosenfeld, D.: Aerosol-cloud-precipitation interactions. Part 1. The nature and sources of cloud-active aerosols, Earth-Sci. Rev., 89, 13–41, doi:10.1016/j.earscirev.2008.03.001, 2008.

Bergstrom, R. W., Pilewskie, P., Russell, P. B., Redemann, J., Bond, T. C., Quinn, P. K., and Sierau, B.: Spectral absorption properties of atmospheric aerosols, Atmos. Chem. Phys., 7, 5937–5943, doi:10.5194/acp-7-5937-2007, 2007.

Bond, T. C., Habib, G., and Bergstrom, R. W.: Limitations in the enhancement of visible light absorption due to mixing state, J. Geophys. Res., 111, D20211, doi:10.1029/2006JD007315, 2006.

Burtscher, H., Baltensperger, U., Bukowiecki, N., Cohn, P., Hüglin, C., Mohr, M., Matter, U., Nyeki, S., Schmatloch, V., Streit, N., and Weingartner, E.: Separation of volatile and non-volatile aerosol fractions by thermodesorption: instrumental development and applications, J. Aerosol Sci., 32, 427–442, doi:10.1016/s0021-8502(00)00089-6, 2001.

Calvert, J.: Hydrocarbon involvement in photochemical smog formation in Los Angeles atmosphere, Environ. Sci. Technol., 10, 256–262, 1976.

Cheng, Y. F., Eichler, H., Wiedensohler, A., Heintzenberg, J., Zhang, Y. H., Hu, M., Herrmann, H., Zeng, L. M., Liu, S., Gnauk, T., Brüggemann, E., and He, L. Y.: Mixing state of elemental carbon and non-light-absorbing aerosol components derived from in situ particle optical properties at Xinken in Pearl River Delta of China, J. Geophys. Res., 111, D20204, doi:10.1029/2005JD006929, 2006.

ACPD

11, 32161–32204, 2011

Cheng, Y. F., Wiedensohler, A., Eichler, H., Heintzenberg, J., Tesche, M., Ansmann, A., Wendisch, M., Su, H., Althausen, D., Herrmann, H., Gnauk, T., Brüggemann, E., Hu, M., and Zhang, Y. H.: Relative humidity dependence of aerosol optical properties and direct radiative forcing in the surface boundary layer at Xinken in Pearl River Delta of China: an observation based numerical study, Atmos. Environ., 42, 6373–6397, 2008a.

Cheng, Y. F., Wiedensohler, A., Eichler, H., Su, H., Gnauk, T., Brüggemann, E., Herrmann, H., Heintzenberg, J., Slanina, J., Tuch, T., Hu, M., and Zhang, Y. H.: Aerosol optical properties and related chemical apportionment at Xinken in Pearl River Delta of China, Atmos. Environ., 42, 6351–6372, 2008b.

Cheng, Y. F., Berghof, M., Garland, R. M., Wiedensohler, A., Wehner, B., Müller, T., Su, H., Zhang, Y. H., Achtert, P., Nowak, A., Pöschl, U., Zhu, T., Hu, M., and Zeng, L. M.: Influence of soot mixing state on aerosol light absorption and single scattering albedo during air mass aging at a polluted regional site in Northeastern China, J. Geophys. Res., 114, D00G10, doi:10.1029/2008jd010883, 2009.

Cooke, W. F. and Wilson, J. J. N.: A global black carbon aerosol model, J. Geophys. Res., 101, 19395–19409, 1996.

Cooke, W. F., Liousse, C., Cachier, H., and Feichter, J.: Construction of a 1° × 1°fossil fuel emission data set for carbonaceous aerosol and implementation and radiative impactor in the ECHAM4 model, J. Geophys. Res., 104, 22137–22162, 1999.

Cooke, W. F., Ramaswamy, V., and Kasibhatla, P.: A general circulation model study of the global carbonaceous aerosol distribution, J. Geophys. Res., 107(D16), 4279, doi:10.1029/2001JD001274, 2002.

Engler, C., Rose, D., Wehner, B., Wiedensohler, A., Brüggemann, E., Gnauk, T., Spindler, G., Tuch, T., and Birmili, W.: Size distributions of non-volatile particle residuals ($D_p < 800$ nm) at a rural site in Germany and relation to air mass origin, Atmos. Chem. Phys., 7, 5785–5802, doi:10.5194/acp-7-5785-2007, 2007.

Frey, A., Rose, D., Wehner, B., Müller, T., Cheng, Y., Wiedensohler, A., and Virkkula, A.: Application of the volatility-TDMA technique to determine the number size distribution and mass concentration of less volatile particles, Aerosol Sci. Tech., 42, 817–828, doi:10.1080/02786820802339595, 2008.

Garland, R. M., Yang, H., Schmid, O., Rose, D., Nowak, A., Achtert, P., Wiedensohler, A., Takegawa, N., Kita, K., Miyazaki, Y., Kondo, Y., Hu, M., Shao, M., Zeng, L. M., Zhang, Y. H., Andreae, M. O., and Pöschl, U.: Aerosol optical properties in a rural environment near the

ACPD
11, 32161–32204, 2011

mega-city Guangzhou, China: implications for regional air pollution, radiative forcing and remote sensing, Atmos. Chem. Phys., 8, 5161–5186, doi:10.5194/acp-8-5161-2008, 2008.
Gunthe, S. S., Rose, D., Su, H., Garland, R. M., Achtert, P., Nowak, A., Wiedensohler, A., Kuwata, M., Takegawa, N., Kondo, Y., Hu, M., Shao, M., Zhu, T., Andreae, M. O., and Pöschl, U.: Cloud condensation nuclei (CCN) from fresh and aged air pollution in the megacity region of Beijing, Atmos. Chem. Phys., 11, 11023–11039, doi:10.5194/acp-11-11023-2011, 2011.
Hasegawa, S. and Ohta, S.: Some measurements of the mixing state of soot-containing particles at urban and non-urban sites, Atmos. Environ., 36, 3899–3908, 2002.
Horvath, H.: Atmospheric light absorption – a review, Atmos. Environ., 27A, 293–317, 1993.
Ivleva, N. P., Messerer, A., Yang, X., Niessner, R., and Pöschl, U.: Raman microspectroscopic analysis of changes in the chemical structure and reactitivity of soot in a diesel exhaust aftertreatment model system, Environ. Sci. Technol., 41, 3702–3707, 2007.
Jacobson, M. Z.: Development and application of a new air pollution modeling system – II. Aerosol module structure and design, Atmos. Environ., 31, 131–144, doi:10.1016/1352-2310(96)00202-6, 1997.
Jacobson, M. Z.: A physically-based treatment of elemental carbon optics: implications for global direct forcing of aerosols, Geophys. Res. Lett., 27, 217–220, 2000.
Jacobson, M. Z.: Strong radiative heating due to the mixing state of black carbon in atmospheric aerosol, Nature, 409, 695–697, 2001.
Japar, S. M., Brachaczek, W. W., Gorse, R. A., Norbeck, J. M., and Pierson, W. R.: The contribution of elemental carbon to the optical properties of rural atmospheric aerosols, Atmos. Environ., 20, 1281–1289, 1986.
Katrinak, K. A., Rez, P., and Buseck, P. R.: Structural variations in individual carbonaceous particles from an urban aerosol, Environ. Sci. Technol., 26, 1967–1976, 1992.
Katrinak, K. A., Rez, P., Perkes, P. R., and Bueseck, P. R.: Fractal geometry of carbonaceous aggregates from an urban aerosol, Environ. Sci. Technol., 27, 539–547, 1993.
Koch, K.: Transport and direct radiative forcing of carbonaceous and sulphate aerosols in the GISS GCM, J. Geophys. Res., 106, 20311–20332, 2001.
Kondo, Y., Komazaki, Y., Miyazaki, Y., Moteki, N., Takegawa, N., Kodama, D., Deguchi, S., Nogami, M., Fukuda, M., Miyakawa, T., Morino, Y., Koike, M., Sakurai, H., and Ehara, K.: Temporal variations of elemental carbon in Tokyo, J. Geophys. Res., 111, D12205, doi:10.1029/2005jd006257, 2006.
Kondo, Y., Sahu, L., Kuwata, M., Miyazaki, Y., Takegawa, N., Moteki, N., Imaru, J., Han, S.,

ACPD
11, 32161–32204, 2011

Nakayama, T., Oanh, N. T. K., Hu, M., Kim, Y. J., and Kita, K.: Stabilization of the mass absorption cross section of black carbon for filter-based absorption photometry by the use of a heated inlet, Aerosol Sci. Tech., 43, 741–756, doi:10.1080/02786820902889879, 2009.
Kondo, Y., Sahu, L., Moteki, N., Khan, F., Takegawa, N., Liu, X., Koike, M., and Miyakawa, T.: Consistency and traceability of black carbon measurements made by laser-induced incandescence, thermal-optical transmittance, and filter-based photo-absorption techniques, Aerosol Sci. Tech., 45, 295–312, doi:10.1080/02786826.2010.533215, 2010.
Lesins, G., Chylek, P., and Lohman, U.: A study of internal and external mixing scenarios and its effect on aerosol optical properties and direct radiative forcing, J. Geophys. Res., 107, 4094, doi:10.1029/2001JD000973, 2002.
Lohmann, U., Feichter, J., Penner, J., and Leaitch, R.: Indirect effect of sulfate and carbonaceous aerosols: a mechanistic treatment, J. Geophys. Res., 105, 12193–12206, 2000.
Moffet, R. C. and Prather, K. A.: In-situ measurements of the mixing state and optical properties of soot with implications for radiative forcing estimates, P. Natl. Acad. Sci. USA, 106, 11872–11877, doi:10.1073/pnas.0900040106, 2009.
Moteki, N., Kondo, Y., Miyazaki, Y., Takegawa, N., Komazaki, Y., Kurata, G., Shirai, T., Blake, D. R., Miyakawa, T., and Koike, M.: Evolution of mixing state of black carbon particles: aircraft measurements over the Western Pacific in March 2004, Geophys. Res. Lett., 34, L11803, doi:10.1029/2006GL028943, 2007.
Novakov, T., Ramanathan, V., Hansen, J. E., Kirchstetter, T. W., Sato, M., Sinton, J. E., and Sathaye, J. A.: Large historical changes of fossil-fuel black carbon aerosols, Geophys. Res. Lett., 30, 1324, doi:10.1029/2002gl016345, 2003.
Orsini, D. A., Wiedensohler, A., and Covert, D. S.: Volatility measurements of atmospheric aerosols in the Mid and South Pacific using a Volatility-Tandem-Differential-Mobility-Analyzer, J. Aerosol Sci., 27, S53–S54, 1996.
Petters, M. D. and Kreidenweis, S. M.: A single parameter representation of hygroscopic growth and cloud condensation nucleus activity, Atmos. Chem. Phys., 7, 1961–1971, doi:10.5194/acp-7-1961-2007, 2007.
Philippin, S., Wiedensohler, A., and Stratmann, F.: Measurements of non-volatile fractions of pollution aerosols with an eight-tube volatility tandem differential mobility analyzer (VTDMA-8), J. Aerosol Sci., 35, 185–203, 2004.
Pöschl, U.: Atmospheric aerosols: composition, transformation, climate and health effects, Angew. Chem. Int. Edit., 44, 7520–7540, doi:10.1002/anie.200501122, 2005.

ACPD
11, 32161–32204, 2011

Pöschl, U., Martin, S. T., Sinha, B., Chen, Q., Gunthe, S. S., Huffman, J. A., Borrmann, S., Farmer, D. K., Garland, R. M., Helas, G., Jimenez, J. L., King, S. M., Manzi, A., Mikhailov, E., Pauliquevis, T., Petters, M. D., Prenni, A. J., Roldin, P., Rose, D., Schneider, J., Su, H., Zorn, S. R., Artaxo, P., and Andreae, M. O.: Rainforest aerosols as biogenic nuclei of clouds and precipitation in the Amazon, Science, 329, 1513–1516, doi:10.1126/science.1191056, 2010.

Riemer, N., Vogel, H., and Vogel, B.: Soot aging time scales in polluted regions during day and night, Atmos. Chem. Phys., 4, 1885–1893, doi:10.5194/acp-4-1885-2004, 2004.

Riemer, N., West, M., Zaveri, R., and Easter, R.: Estimating black carbon aging time-scales with a particle-resolved aerosol model, J. Aerosol Sci., 41, 143–158, doi:10.1016/j.jaerosci.2009.08.009, 2010.

Rose, D., Wehner, B., Ketzel, M., Engler, C., Voigtländer, J., Tuch, T., and Wiedensohler, A.: Atmospheric number size distributions of soot particles and estimation of emission factors, Atmos. Chem. Phys., 6, 1021–1031, doi:10.5194/acp-6-1021-2006, 2006.

Rose, D., Gunthe, S. S., Mikhailov, E., Frank, G. P., Dusek, U., Andreae, M. O., and Pöschl, U.: Calibration and measurement uncertainties of a continuous-flow cloud condensation nuclei counter (DMT-CCNC): CCN activation of ammonium sulfate and sodium chloride aerosol particles in theory and experiment, Atmos. Chem. Phys., 8, 1153–1179, doi:10.5194/acp-8-1153-2008, 2008.

Rose, D., Gunthe, S. S., Su, H., Garland, R. M., Yang, H., Berghof, M., Cheng, Y. F., Wehner, B., Achtert, P., Nowak, A., Wiedensohler, A., Takegawa, N., Kondo, Y., Hu, M., Zhang, Y., Andreae, M. O., and Pöschl, U.: Cloud condensation nuclei in polluted air and biomass burning smoke near the mega-city Guangzhou, China – Part 2: Size-resolved aerosol chemical composition, diurnal cycles, and externally mixed weakly CCN-active soot particles, Atmos. Chem. Phys., 11, 2817–2836, doi:10.5194/acp-11-2817-2011, 2011.

Rosen, H., Hansen, A. D. A., Gundel, L., and Novakov, T.: Identification of the optical absorbing component in urban aerosols, Appl. Optics, 17, 3859–3861, 1979.

Sadezky, A., Muckenhuber, H., Grothe, H., Niessner, R., and Pöschl, U.: Raman microspectroscopy of soot and related carbonaceous materials: spectral analysis and structural information, Carbon, 43, 1731–1742, doi:10.1016/j.carbon.2005.02.018, 2005.

Seinfeld, J. H. and Pandis, S. N.: Atmospheric Chemistry and Physics, from Air Pollution to Climate Change, Wiley, New York, 2006.

Shiraiwa, M., Kondo, Y., Moteki, N., Takegawa, N., Miyazaki, Y., and Blake, D. R.: Evolution

ACPD
11, 32161–32204, 2011

of mixing state of black carbon in polluted air from Tokyo, Geophys. Res. Lett., 34, L16803, doi:10.1029/2007GL029819, 2007.
Shiraiwa, M., Kondo, Y., Moteki, N., Takegawa, N., Sahu, L. K., Takami, A., Hatakeyama, S., Yonemura, S., and Blake, D. R.: Radiative impact of mixing state of black carbon aerosol in Asian outflow, J. Geophys. Res., 113, D24210, doi:10.1029/2008jd010546, 2008.
Shiraiwa, M., Kondo, Y., Iwamoto, T., and Kita, K.: Amplification of light absorption of black carbon by organic coating, Aerosol Sci. Tech., 44, 46–54, doi:10.1080/02786820903357686, 2010.
Smith, D. M., Akhter, M. S., Jassim, J. A., Sergides, C. A., Welch, W. F., and Chughtai, A. R.: Studies of the stucture and reactivity of soot, Aerosol Sci. Tech., 45, 1397–1415, 1989.
Smith, M. H. and O'Dowd, C. D.: Observations of accumulation mode aerosol composition and soot carbon concentrations by means of a high-temperature volatility technique, J. Geophys. Res., 101, 19583–19591, doi:10.1029/95jd01750, 1996.
Stephens, M., Turner, N., and Sandberg, J.: Particle identification by laser-induced incandescence in a solid-state laser cavity, Appl. Optics, 42, 3726–3736, 2003.
Su, H., Rose, D., Cheng, Y. F., Gunthe, S. S., Massling, A., Stock, M., Wiedensohler, A., Andreae, M. O., and Pöschl, U.: Hygroscopicity distribution concept for measurement data analysis and modeling of aerosol particle mixing state with regard to hygroscopic growth and CCN activation, Atmos. Chem. Phys., 10, 7489–7503, doi:10.5194/acp-10-7489-2010, 2010.
Takegawa, N., Miyakawa, T., Kondo, Y., Jimenez, J. L., Zhang, Q., Worsnop, D. R., and Fukuda, M.: Seasonal and diurnal variations of submicron organic aerosol in Tokyo observed using the Aerodyne serosol mass spectrometer, J. Geophys. Res., 111, D11206, doi:10.1029/2005JD006515, 2006.
Takegawa, N., Miyakawa, T., Watanabe, M., Kondo, Y., Miyazaki, Y., Han, S., Zhao, Y., van Pinxteren, D., Bruggemann, E., Gnauk, T., Herrmann, H., Xiao, R., Deng, Z., Hu, M., Zhu, T., and Zhang, Y.: Performance of an aerodyne aerosol mass spectrometer (AMS) during intensive campaigns in China in the summer of 2006, Aerosol Sci. Tech., 43, 189–204, 2009.
Tsigaridis, K. and Kanakidou, M.: Global modelling of secondary organic aerosol in the troposphere: a sensitivity analysis, Atmos. Chem. Phys., 3, 1849–1869, doi:10.5194/acp-3-1849-2003, 2003.
Wehner, B., Berghof, M., Cheng, Y. F., Achtert, P., Birmili, W., Nowak, A., Wiedensohler, A., Garland, R. M., Pöschl, U., Hu, M., and Zhu, T.: Mixing state of nonvolatile aerosol particle

ACPD
11, 32161–32204, 2011

fractions and comparison with light absorption in the polluted Beijing region, J. Geophys. Res., 114, D00G17, doi:10.1029/2008jd010923, 2009.

Wiedensohler, A., Cheng, Y. F., Nowak, A., Wehner, B., Achtert, P., Berghof, M., Birmili, W., Wu, Z. J., Hu, M., Zhu, T., Takegawa, N., Kita, K., Kondo, Y., Lou, S. R., Hofzumahaus, A., Holland, F., Wahner, A., Gunthe, S. S., Rose, D., Su, H., and Pöschl, U.: Rapid aerosol particle growth and increase of cloud condensation nucleus activity by secondary aerosol formation and condensation: a case study for regional air pollution in Northeastern China, J. Geophys. Res., 114, D00G08, doi:10.1029/2008jd010884, 2009.

Xie, X., Shao, M., Liu, Y., Lu, S., Chang, C.-C., and Chen, Z.-M.: Estimation of initial isoprene contribution to ozone formation potential in Beijing, China, Atmos. Environ., 42, 6000–6010, doi:10.1016/j.atmosenv.2008.03.035, 2008.

Zhang, R., Khalizov, A. F., Pagels, J., Zhang, D., Xue, H., and McMurry, P. H.: Variability in morphology, hygroscopicity, and optical properties of soot aerosols during atmospheric processing, P. Natl. Acad. Sci. USA, 105, 10291–10296, doi:10.1073/pnas.0804860105, 2008.

Zhou, Y., Wu, Y., Yang, L., Fu, L., He, K., Wang, S., Hao, J., Chen, J., and Li, C.: The impact of transportation control measures on emission reductions during the 2008 olympic games in Beijing, China, Atmos. Environ., 44, 285–293, doi:10.1016/j.atmosenv.2009.10.040, 2010.

ACPD

11, 32161–32204, 2011

Table 1. Statistics of F_{in} at different diameters (429 data points).

F_{in}	30 nm	50 nm	100 nm	150 nm	200 nm	260 nm	320 nm
Arithmetic mean	0.80	0.74	0.70	0.64	0.60	0.62	0.57
Standard deviation	0.075	0.078	0.084	0.090	0.100	0.100	0.102

ACPD
11, 32161–32204, 2011

Table 2. Correlation matrix of F_{in} at different diameters (429 data points).

R	30 nm	50 nm	100 nm	150 nm	200 nm	260 nm
50 nm	0.49					
100 nm	−0.12	0.40				
150 nm	−0.09	0.25	0.86			
200 nm	−0.04	0.24	0.73	0.93		
260 nm	−0.01	0.24	0.65	0.87	0.95	
320 nm	0.00	0.28	0.58	0.80	0.89	0.94

ACPD
11, 32161–32204, 2011

Table 3. Correlation of measured and predicted F_{in} (429 data points for individual size bins; 2145 data points for all size bins).

	D_p					
	100 nm	150 nm	200 nm	260 nm	320 nm	all
k^*	0.99 ± 0.01	1.01 ± 0.00	1.02 ± 0.01	0.96 ± 0.01	1.00 ± 0.01	0.99
R^2	0.75	1.00	0.80	0.68	0.41	0.77

*k is the fit parameter in the equation: F_{in} (predicted) = kF_{in} (measured).

ACPD
11, 32161–32204, 2011

Table A1. Acronyms.

Symbol	Description
AMS	Aerosol mass spectrometer
ATOFMS	Aerosol time-of-flight mass spectrometer
CAREBeijing	Campaign of air quality research in Beijing
CCN	Cloud condensation nuclei
DMA	Differential mobility analyzer
EC	Elemental carbon
GC-PID	Gas chromatography-photo ionization detector
OC	Organic carbon
PAN	Peroxyacetyl nitrates
PM_1	Particles of 1 µm or less in aerodynamic diameter
PM_{10}	Particles of 10 µm or less in aerodynamic diameter
SP2	Single particle soot photometer
Soot (NVP)	Non-volatile-core containing particles, measured by the VTDMA, and taken as soot particles
VTDMA	Volatility tandem differential mobility analyzer

ACPD
11, 32161–32204, 2011

Table A2. Symbols.

Symbol	Unit*	Quantity
D	$m^2\ s^{-1}$	Diffusion coefficient for species in air
D_p	nm	Dry particle diameter
$D_{p,300\,°C}$	nm	Particle diameter after being heated at 300 °C in the VTDMA
[E]	ppb	Concentration of ethylbenzene
[EC]	$\mu g\ m^{-3}$	Concentration of elemental carbon
$Emis_{in}$	$cm^{-3}\ h^{-1}$	Number emission rate of internally mixed soot particles
$Emis_{tot}$	$cm^{-3}\ h^{-1}$	Number emission rate of all soot particles
$Emis_{tot,m}$	$\mu g\ m^{-3}\ h^{-1}$	Mass emission rate of all soot particles
F_{in}		Number fraction of internally mixed soot particles (medium volatile particles measured by VTDMA with $82\,\% > D_{p,300\,°C}/D_p > 45\,\%$) in total soot particles
$f(Kn, \alpha)$		Correction due to non-continuum effects and imperfect surface accommodation
[IM]	$\mu g\ m^{-3}$	$[IM]=[NH_4^+]+[NO_3^-]+[SO_4^{2-}]+[Cl^-]$ (inorganic mass in PM_1 measured by aerosol mass spectrometer, AMS)
Kn		Knudsen number
$k_{ex\rightarrow in}$	h^{-1}	Turnover rate of soot, the rate of conversion of externally mixed to internally mixed soot
k_{shift}	nm^{-2}	Parameter representing the rate of change of particle number concentrations at certain size bin due to the condensational growth
$k_{ex,shift}$	nm^{-2}	k_{shift} of externally mixed soot particles
$k_{in,shift}$	nm^{-2}	k_{shift} of internally mixed soot particles
M	$kg\ mol^{-1}$	Molecular weight
$[NO_x]$	ppb	Concentration of $NO + NO_2$
$[NO_y]$	ppb	Concentration of total reactive nitrogen
$[NO_z]$	ppb	$[NO_y]$-$[NO_x]$
n_{in}	cm^{-3}	Number concentration of internally mixed soot particles
n_{ex}	cm^{-3}	Number concentration of externally mixed soot particles
n_{tot}	cm^{-3}	Number concentration of total soot particles
[OM]	$\mu g\ m^{-3}$	Mass concentration of organic matter (in PM_1 measured by aerosol mass spectrometer, AMS)
P	Pa	Supersaturated vapor pressure of condensable species
R	$J\ mol^{-1}\ K^{-1}$	Molar gas constant (unless specified)
S	%	Supersaturation of water vapor
T	K	Kelvin temperature
t	s	Time
[X]	ppb	Concentration of m,p-xylene
α		Accommodation coefficient
β		$\beta = Emis_{in}/Emis_{tot}$
$\sigma_{g,\kappa}$		Geometric standard deviation in a lognormal κ distribution
κ		Hygroscopicity parameter
λ	m	Mean free path of the condensable species in air
ε		Conversion coefficient of the growing to shrinking speed for externally mixed soot particles
ρ_p	$kg\ m^{-3}$	Particle density

* if not specified.

ACPD
11, 32161–32204, 2011

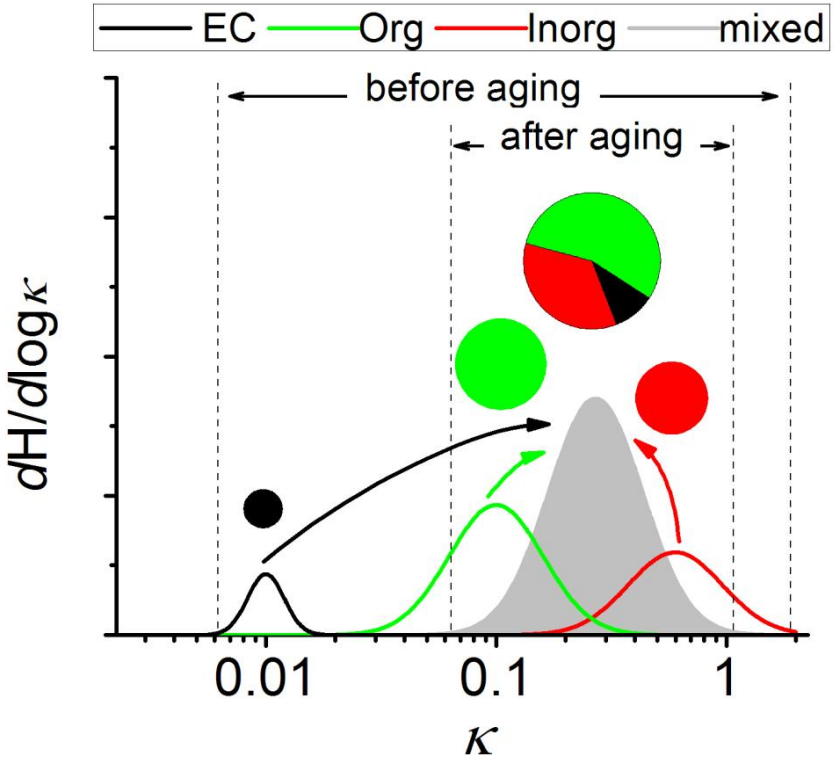

Fig. 1. Evolution of the mixing state and hygroscopicity (κ) in the aging process. Solid lines refer to $dH/d\log\kappa$, the normalized number distributions of particle hygroscopicity. The areas of the pie diagrams refer to the abundance of individual chemical components (EC: elemental carbon, Org: organics, Inorg: inorganics). After aging, the externally mixed particles become internally mixed (coated).

ACPD
11, 32161–32204, 2011

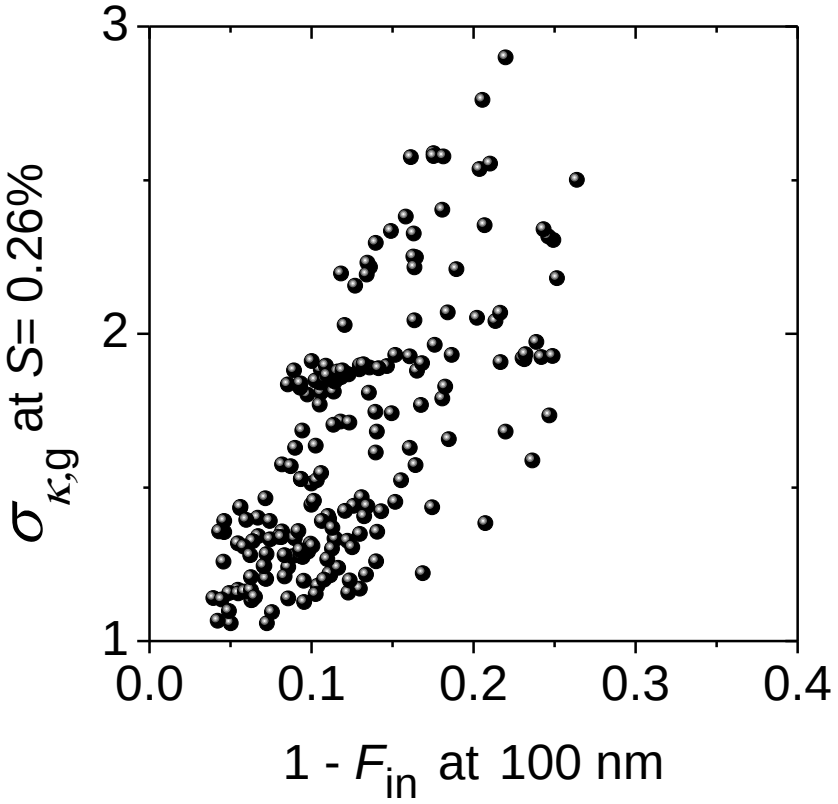

Fig. 2. Comparison of aerosol and soot (NVP) mixing state parameters during the CAREBeijing-2006 campaign. The parameter $\sigma_{\kappa,g}$ was calculated from the aerosol hygroscopicity (i.e., κ) distribution measured at supersaturation $S = 0.26\,\%$ (Su et al., 2010); and the $(1 - F_{in})$ was determined for particles of diameters at 100 nm by the VTDMA measurements. Note that the mean activation diameter observed at $S = 0.26\,\%$ is 85 nm (Gunthe et al., 2011).

ACPD
11, 32161–32204, 2011

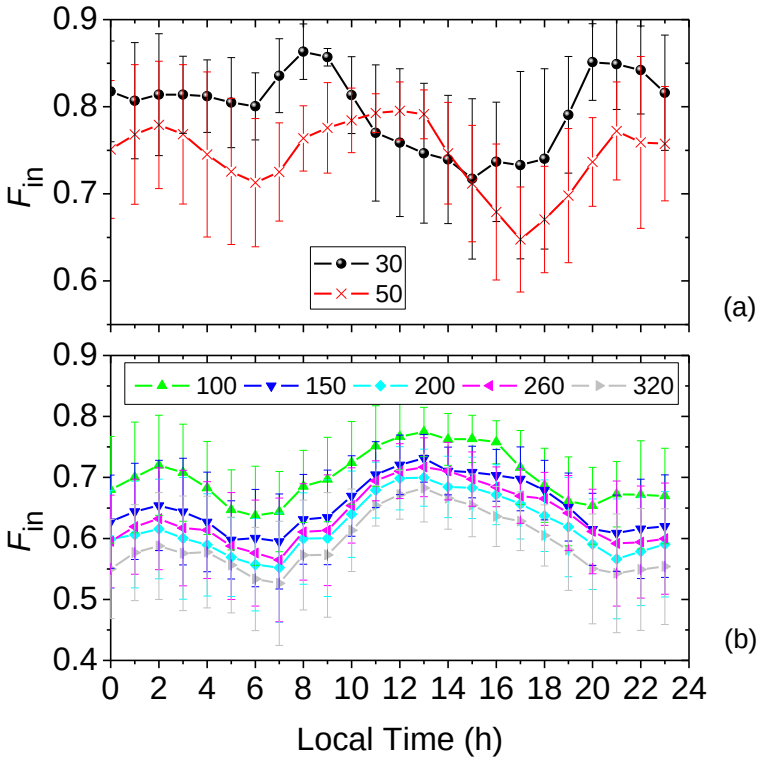

Fig. 3. Average diurnal variation of F_{in} at different size bins (30, 50, 100, 150, 200, 260, and 320 nm). Symbols represent arithmetic mean values and error bars represent the standard deviation. Since transport might significantly affect the evolution of F_{in} days with average wind speed $> 2\,m\,s^{-1}$ (20, 22 August, 3, 4, 5, 6 and 8 September) were completely removed in the analyses.

ACPD
11, 32161–32204, 2011

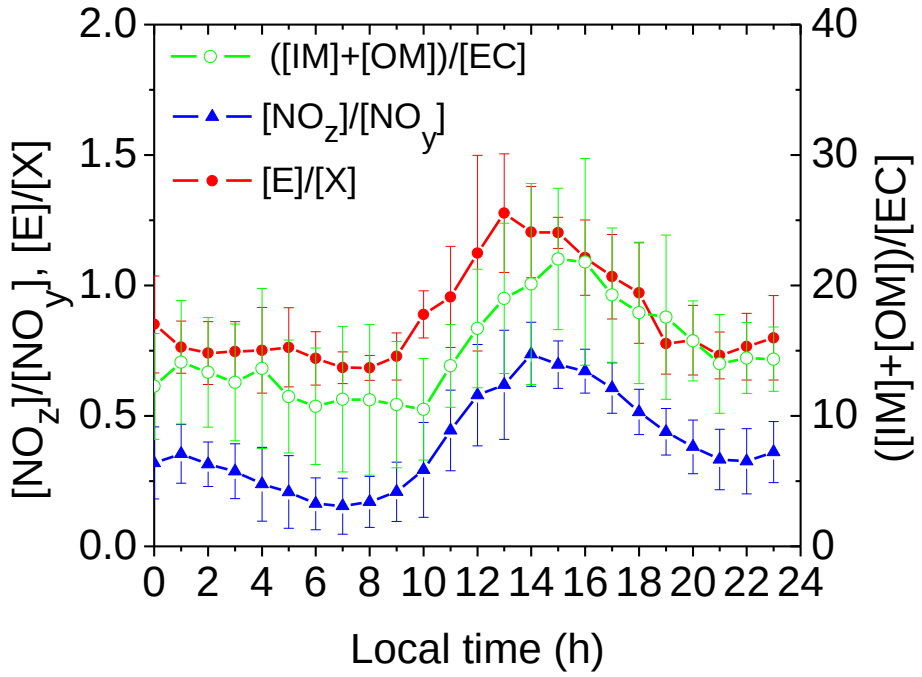

Fig. 4. Averaged diurnal variation of [NO_z]/[NO_y], [E]/[X] and ([IM] + [OM])/[EC]. Symbols represent arithmetic mean values and error bars represent the standard deviation.

ACPD
11, 32161–32204, 2011

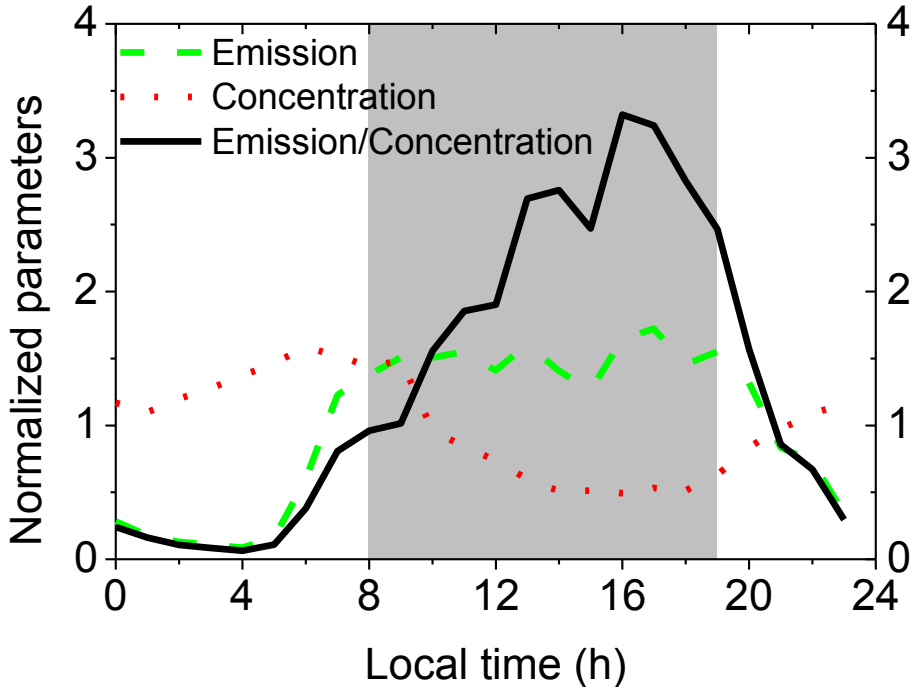

Fig. 5. Diurnal variation of normalized parameters: (a) emission rates from traffic in Beijing (according to CO emission intensity in the work of Zhou et al., 2010) (green dashed lines); (b) EC concentrations measured by an online Sunset EC/OC analyzer (red dotted lines); and (c) ratio of emission rate to EC concentration (black solid lines). Shaded areas represent the time period of 8:00–19:00 LT when vertical mixing is supposed to significantly affect EC concentrations.

ACPD
11, 32161–32204, 2011

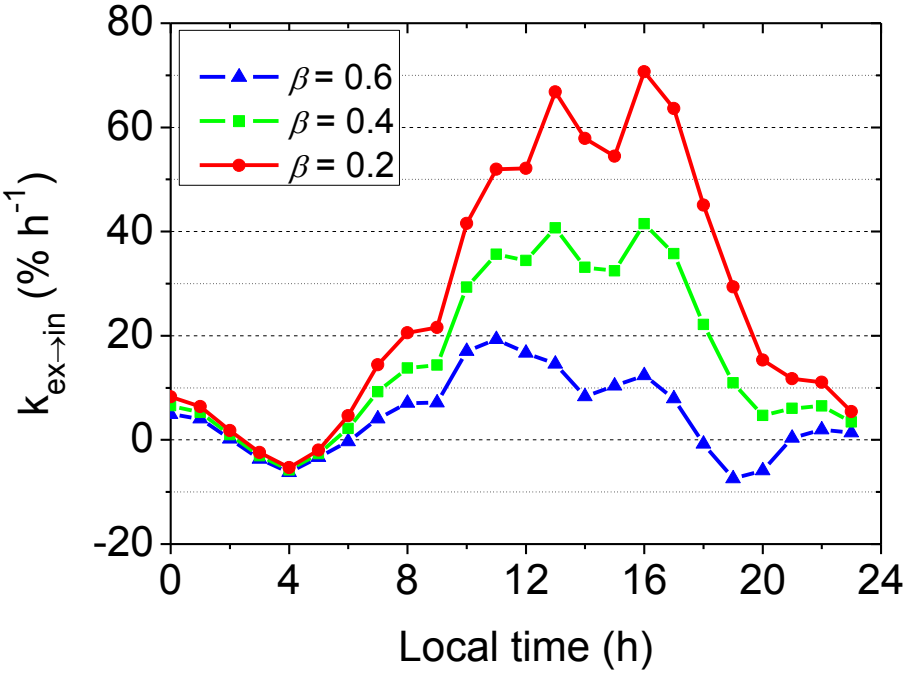

Fig. 6. The actual turnover rate of soot (NVP), $k_{ex \rightarrow in}$, assuming different emission factors β (number fraction of internally mixed soot particles to total soot particles in the emissions).

ACPD
11, 32161–32204, 2011

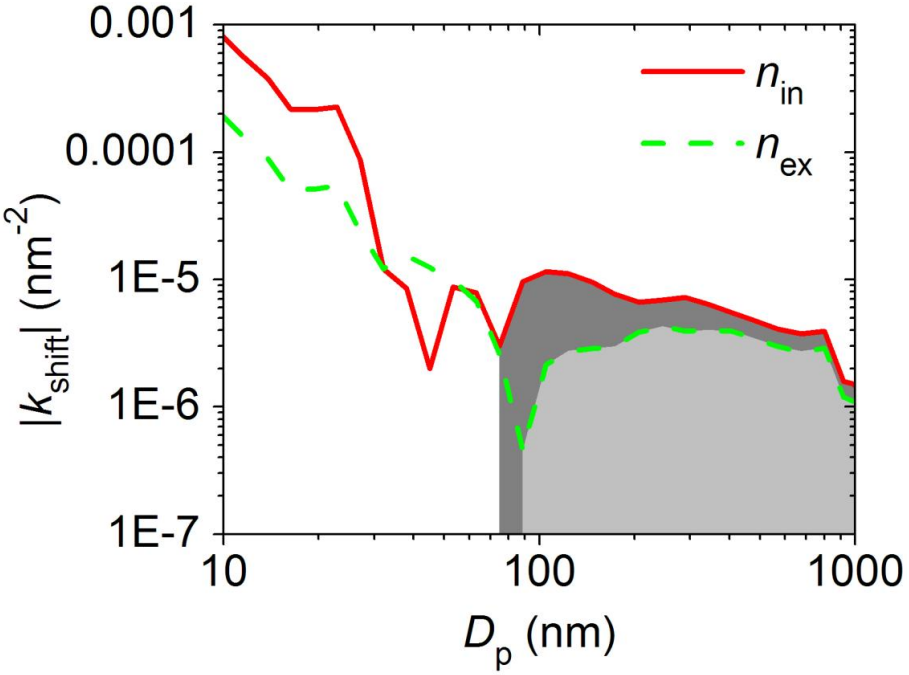

Fig. 7. The size dependence of the particle size distribution $n(D_p)$ variation due to condensation growth. k_{shift} equals $(\partial n/\partial t)/n$ due to condensation growth divided by a constant (in Eq. 20). k_{shift} can either be positive or negative, which indicates increases and decreases of $n(D_p)$ due to condensation growth, respectively. The shaded areas (with gray and light gray for n_{in} and n_{ex}, respectively) indicate the size ranges where k_{shift} are positive while k_{shift} are negative in the un-shaded ranges.

ACPD
11, 32161–32204, 2011

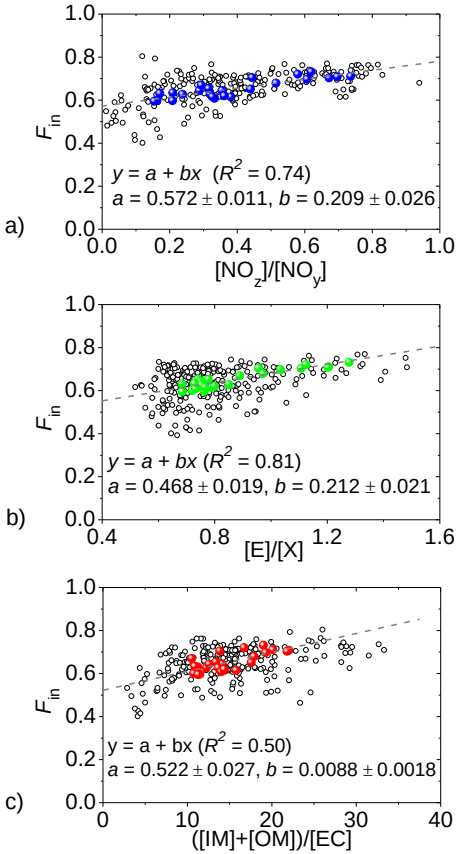

Fig. 8. Correlations between F_{in} and **(a)** [NO$_z$]/[NO$_y$], **(b)** [E]/[X], and **(c)** ([IM] + [OM])/[EC]. The open circles are measurement data with a time resolution of 1 h; while the colored solid dots are average diurnal data. The average diurnal data can be linearly fitted by equation "$y = a + bx$" (dashed line) with R being the correlation coefficient.

ACPD
11, 32161–32204, 2011

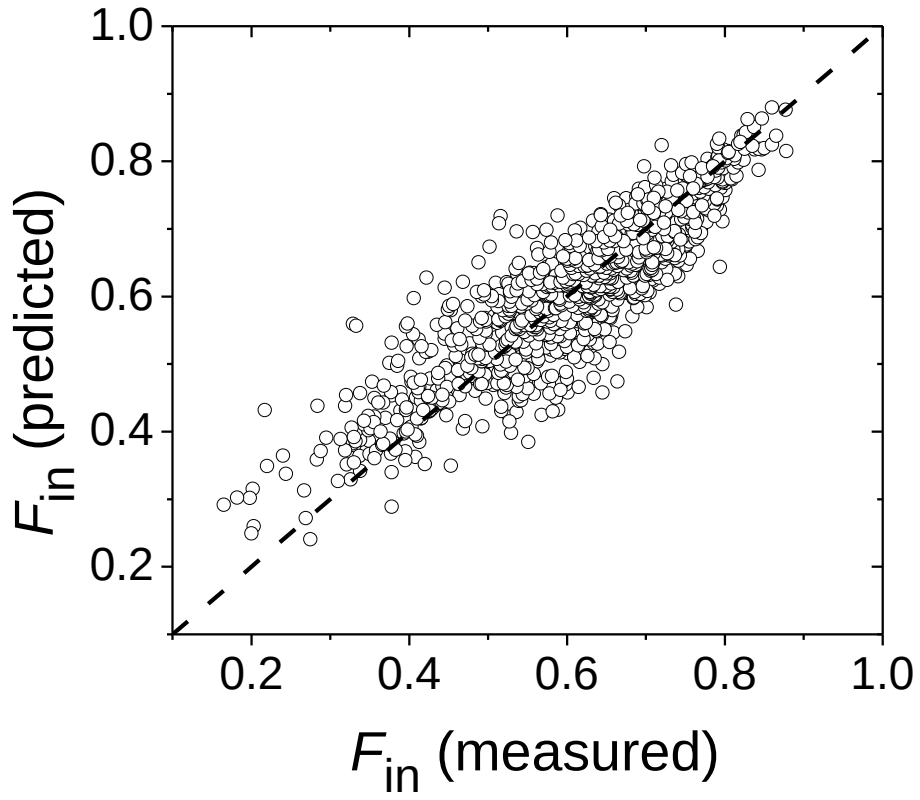

Fig. 9. Measured and predicted F_{in} over 100 nm to 320 nm (2145 data points). The dashed line represents the 1 : 1 line.

ACPD
11, 32161–32204, 2011